JACS
JOURNAL OF THE AMERICAN CHEMICAL SOCIETY
Communication
pubs.acs.org/JACS

Photocarrier Recombination Dynamics in Perovskite $CH_3NH_3PbI_3$ for Solar Cell Applications

Yasuhiro Yamada,* Toru Nakamura, Masaru Endo, Atsushi Wakamiya, and Yoshihiko Kanemitsu*

Institute for Chemical Research, Kyoto University, Uji, Kyoto 611-0011, Japan

ABSTRACT: Using time-resolved photoluminescence and transient absorption measurements at room temperature, we report excitation-intensity-dependent photocarrier recombination processes in thin films made from the organo-metal halide perovskite semiconductor $CH_3NH_3PbI_3$ for solar-cell applications. The photocarrier dynamics are well described by a simple rate equation including single-carrier trapping and electron−hole radiative recombination. This result provides clear evidence that the free-carrier model is better than the exciton model for interpreting the optical properties of $CH_3NH_3PbI_3$. The observed large two-carrier recombination rate suggests the promising potential of perovskite semiconductors for optoelectronic device applications. Our findings provide the information about the dynamical behaviors of photoexcited carriers that is needed for developing high-efficiency perovskite solar cells.

Halide-based perovskite semiconductors $CH_3NH_3PbX_3$ [X = Cl, Br, or I] have recently attracted increasing attention due to their advanced optoelectronic properties for device applications such as photovoltaic cells and light-emitting devices.[1−8] Perovskite-based solar cells, which combine high efficiency, low cost, and high flexibility, were originally developed from a type of sensitized solar cells, in which the halide perovskite semiconductors are used as light-harvesting sensitizers.[1−5] More recently, planar heterostructured perovskite solar cells were also developed, implying that the working principle of perovskite solar cells is quite different from that of conventional sensitized solar cells.[6,9] The power conversion efficiency (PCE) of perovskite solar cells currently reaches values of nearly 20%, which is almost twice as large as that in the most efficient sensitized solar cells.[10,11] For this reason, it is important to determine the key features that provide the high PCE of perovskite solar cells. It has been noted that $CH_3NH_3PbX_3$ displays a long carrier diffusion length[12,13] and ambipolar carrier conduction;[14] these effects would be expected to serve as the dominant mechanisms supporting the high performance of perovskite solar cells. The estimation of the carrier diffusion length is based on a time-resolved photoluminescence (PL) analysis under the assumption of a one-dimensional exciton diffusion model.[12,13] However, this explanation still left unsettled and under active discussion whether it is the exciton or the free-carrier model that is more appropriate for interpreting optical properties in perovskite semiconductors. The optimal device structures and efficiency-determining factors strongly depend on whether excitons or free carriers are dominant.[15]

Moreover, even the fundamental properties of photoexcited states in halide perovskite semiconductors remain unclear, and this prevents us from attaining a deeper understanding of the photovoltaic properties. Since the photoconversion processes are driven by transiently photoexcited electrons and holes, it is necessary to study the dynamical optical properties. We have previously reported the static near-band-edge optical properties of $CH_3NH_3PbI_3$ and accurately determined the direct band gap energy of $CH_3NH_3PbI_3$ on mesoporous TiO_2 electrodes to be 1.61 eV.[16] Based on the above research, in this work, we combine time-resolved PL and TA measurements in order to gain a deeper understanding of the dynamical behavior of photocarriers.[17]

In order to deposit the perovskite layer, we used a sequential deposition method in an inert glovebox (Ar; H_2O and O_2, < 0.1 ppm) using dehydrated (H_2O, < 8 ppm) solvents and PbI_2 (H_2O, < 100 ppm). Our method using dehydrated materials[18] enables the highly reproducible fabrication of solar cells. A typical I−V characteristic of our solar cell device is shown in Figure 1a. The obtained short-circuit current (J_{SC}), open-circuit

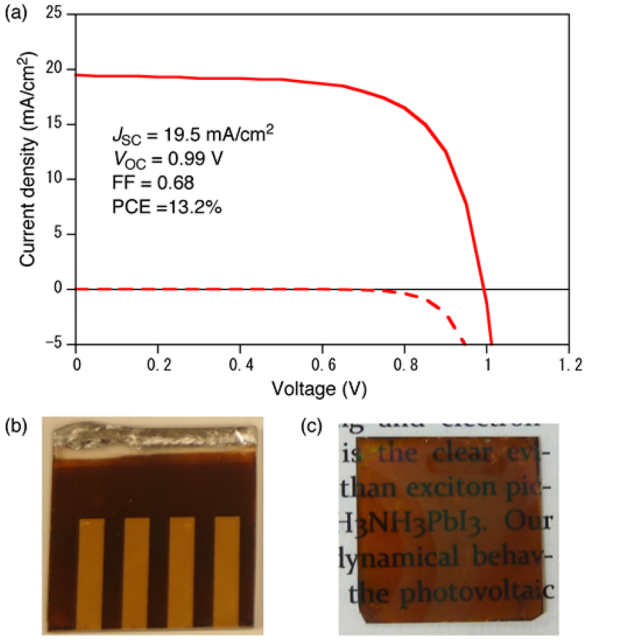

Figure 1. (a) Photocurrent density−voltage curves of perovskite-based solar cells. Photographic top view of (b) a solar cell and (c) a thin perovskite sample on a glass plate.

Received: July 2, 2014
Published: July 30, 2014

dx.doi.org/10.1021/ja506624n | J. Am. Chem. Soc. 2014, 136, 11610−11613

voltage (V_{OC}), and fill factor (FF) were 19.5 mA/cm^2, 0.99 V, and 0.68, respectively. The PCE was 13.2%. In a similar manner, we fabricated a thin layer of perovskite on a glass plate. Thus, PbI_2 was deposited on the plate by spin-coating a solution of PbI_2 in DMF (1.0 M) at 70 °C. After annealing (70 °C, 1 h), the film was dipped for 40 s in a 0.06 M solution of CH_3NH_3I in 2-propanol to produce a thin layer of red-black perovskite (see Figure 1b). The film thickness was estimated to be 280 nm by scanning electron microscopy (SEM) measurement. Samples were kept in transparent acryl boxes filled with argon gas before and during measurements to keep the samples from being exposed to air in order to prevent degradation caused by oxygen and humidity. Before the experiments, the samples were left in the boxes for more than 3 days after fabrication to allow the material properties to stabilize. The need for such a stabilization procedure has been mentioned in previous reports.[12]

Time-resolved PL measurements were conducted with a monochromator and a streak camera. The time resolution of PL measurements was 20 ps. The femtosecond TA measurements were carried out with a standard white-light pump–probe method. The light source was a wavelength-tunable femtosecond laser system (pulse width: 300 fs, repetition rate: 50 kHz). The excitation photon energy was fixed at 1.8 eV. All experiments were conducted at room temperature.

Figure 2 shows the two-dimensional (2D) contour image of a typical time-resolved PL spectrum of a $CH_3NH_3PbI_3$ thin film

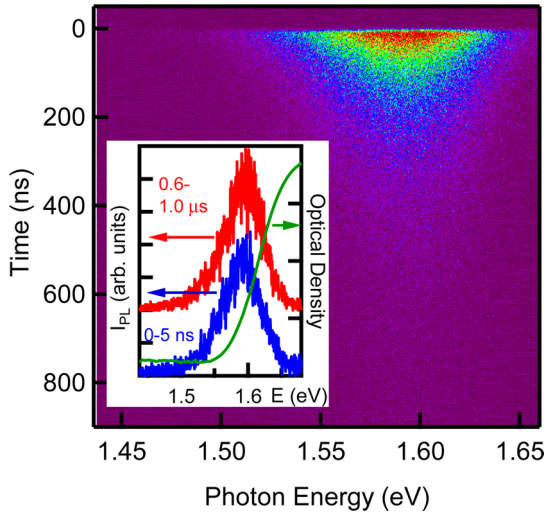

Figure 2. Two-dimensional contour image of time-resolved PL spectra for a $CH_3NH_3PbI_3$ film. The inset shows the PL spectra at different delay times under an excitation of 200 nJ/cm^2. The optical density spectrum is also plotted.

at room temperature under an excitation of 200 nJ/cm^2. The PL peak is located at 1.59 eV, and the shape of the spectrum is independent of the time elapsed after excitation, as shown in the inset. The inset shows the results of integrating the PL spectra between 0.6 and 1.0 μs and between 0 and 5 ns, as indicated by the red and blue lines, respectively. The PL intensity was normalized, and the two spectra were offset from one another for clarity. The optical absorption spectrum is also plotted in the same figure in green. The near-band-edge optical absorption has no excitonic peak structure at room temperature and shows an abrupt increase in the absorption coefficient that is typically observed in direct-gap semiconductors. The PL spectrum has no significant Stokes shift, indicating that the PL reflects the recombination of band-edge electrons and holes (free excitons or free carriers). Also, we confirmed that the shape of the PL spectrum is independent of the excitation intensity and photon energy, as reported by previous studies.[8] We used this band-edge PL as a probe to study the carrier recombination and relaxation dynamics in $CH_3NH_3PbI_3$ thin films.

Figure 3a shows the PL decay dynamics under different excitation intensities monitored at 1.59 eV. The PL intensity

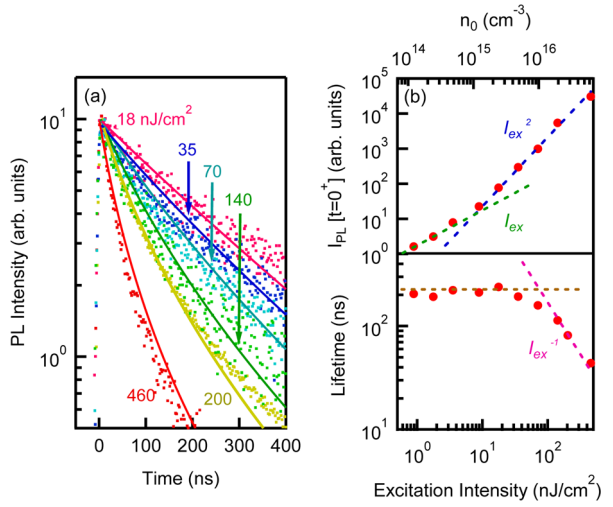

Figure 3. (a) PL dynamics of a $CH_3NH_3PbI_3$ film under different excitation intensities. (b) Excitation-intensity dependence of the PL intensity and effective PL lifetime. The initial photocarrier density n_0 is shown along the top axis. The dotted lines are intended to help guide the eye.

was normalized to the peak intensity for comparison. Under excitation intensities of less than 20 nJ/cm^2, the PL dynamics display a slow and nearly monoexponential decay profile with a lifetime of ~140 ns. When the excitation intensity exceeds 20 nJ/cm^2, a fast and nonexponential component appears.

Figure 3b summarizes the effective PL lifetime and PL intensity just after the excitation as a function of excitation intensity. The initial photocarrier density calculated using the optical absorption coefficient in ref 12 is also shown on the top axis of this figure (where the optical penetration depth at 1.8 eV is 250 nm). The effective PL lifetime $t_{1/e}$ is defined by $I_{PL}(t_{1/e}) = I_{PL}(0)/e$, where $I_{PL}(t)$ represents the PL decay dynamics. We examined another typical definition of $t_{1/e}$, $\int_0^{t_{1/e}} I_{PL}(t)\,dt = \int_0^{\infty} I_{PL}(t)\,dt/e$, and confirmed that similar results are obtained using this definition. The PL intensity just after the excitation shows a quadratic dependence on the excitation intensity for values above 20 nJ/cm^2. The two-photon absorption process is not relevant to this power dependence, as will be discussed later. This result means that the origin of the PL is a radiative two-carrier (nongeminate) recombination process involving electrons and holes,[19] but not excitons. Considering the small Stokes shift of the energy associated with the peak of the PL spectrum, we can conclude that the band-to-band radiative recombination between free electrons in the conduction band and free holes in the valence band occurs in $CH_3NH_3PbI_3$.

Below excitation intensities of 20 nJ/cm^2, the PL intensity has a linear dependence on the excitation intensity. It should be noted that the shape of the PL spectrum in such a weak-

dx.doi.org/10.1021/ja506624n | J. Am. Chem. Soc. 2014, 136, 11610–11613

excitation regime is the same as that under strong excitation, indicating that the PL mechanism is the same for these excitation regimes. Therefore, we can conclude that the recombination of photoexcited carriers and unintentionally doped carriers in the sample is the dominant light-emission mechanism under weak excitation. The photocarrier density at the crossover point ($\sim 1 \times 10^{15}$ cm^{-3}) corresponds to the carrier density resulting from unintentional doping in this sample.

The PL lifetime decreases in inverse proportion to the excitation intensity at excitations above 20 nJ/cm^2, while it stays almost constant under weak excitation. This also indicates that the two-carrier recombination process is dominant under strong excitation. Such power-dependent dynamics are well explained by a simple rate equation that includes single-carrier trapping and two-carrier (electron−hole) radiative recombination:

$$dn/dt = -A_n n - Bnp \quad (1a)$$

$$dp/dt = -A_p p - Bnp \quad (1b)$$

$$I_{PL} \propto Bnp + BN_e p + BN_p n \quad (1c)$$

Here n and p are the photoexcited electron and hole densities. A_n, A_p, and B represent the electron trapping rate, the hole trapping rate, and the two-carrier radiative recombination coefficient, respectively. N_e and N_p are the electron and hole densities caused by unintentional doping in the sample. Because photoexcitation produces equal numbers of electrons and holes (i.e., $n = p$), the above equations can be simplified to $dn/dt = -An - Bn^2$ and $I_{PL} \propto Bn^2 + BNn$, where $A = (A_n + A_p)/2$ and $N = N_e + N_p$. When the photocarrier density (n) is much larger than the carrier density from unintentional doping (N),[19] the effective PL lifetime can be approximately written as $t_{1/e} = 1/(A + Bn_0)$, where n_0 is the photocarrier density just after the excitation. This expression reproduces well the experimental results shown in Figure 3b.

We performed global fitting of the PL dynamics shown in Figure 3a to the rate equations. The fitting results are shown in Figure 3a as solid lines; from this fit, we obtained the values $A = 1.8 \times 10^7$ s^{-1} and $B = 1.7 \times 10^{-10}$ s^{-1} cm^3. The radiative recombination coefficient B for $CH_3NH_3PbI_3$ is comparable to that in typical direct-gap semiconductors (e.g., GaAs: $B \approx 7.2 \times 10^{-10}$ s^{-1} cm^3).[20] Such a high B coefficient is caused by the direct allowed interband optical transition. Also, a large oscillator strength is theoretically predicted for the band-to-band transition, which is comparable to those in conventional III−V semiconductors such as GaAs.[21] This result indicates a promising potential for optoelectronic device applications such as light-emitting devices and lasers. The high B coefficient can account for the lasing effect in $CH_3NH_3PbI_3$.[8]

It should be noted that the A coefficient is sensitive to small differences in the sample fabrication conditions; this parameter ranges from 1.3 to 1.9×10^{-10} s^{-1} cm^3 in our experiments. The typical A coefficient (which represents the PL decay rate under weak excitation) in our sample is much smaller than that previously reported.[12,13] This suggests that our sample is of high quality and has fewer carrier-trapping centers such as defects and impurities compared with the samples in previous reports.

To confirm our carrier recombination model, TA spectroscopy was also performed. Figure 4a shows the optical density change (ΔOD) caused by pump excitation under different

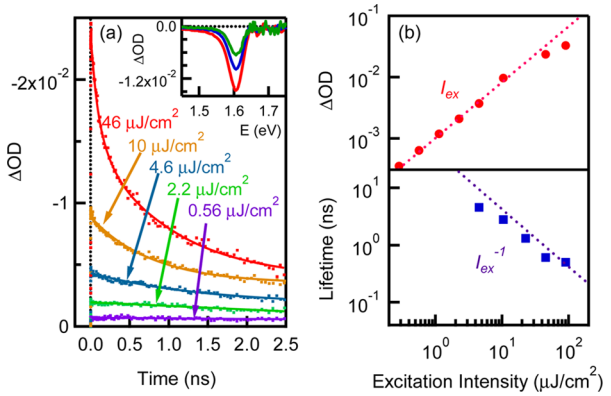

Figure 4. (a) TA dynamics of a $CH_3NH_3PbI_3$ film under different excitation intensities. The inset shows the TA spectra at different delay times (0−0.4 ns, 0.9−1.3 ns, and 2.2−2.4 ns). (b) Excitation-intensity dependence of the TA intensity and effective TA lifetime.

excitation intensities. As shown in the inset of Figure 4a, the TA spectrum shows a dip at 1.61 eV (which is approximately equal to the band gap energy[16]) that is caused by photobleaching, and the shape of the spectrum is independent of delay time, photon energy, and intensity. The bleaching-signal intensity reflects the band-edge photocarrier density. We monitored the temporal change in TA at 1.61 eV. The TA signal rises just after the excitation within a pulse width ($\sim$300 fs), which means that the intraband carrier relaxation occurs on a very short time scale and is consistent with the previous reports.[13] As with the PL dynamics, the TA dynamics show a strong excitation-intensity dependence: the TA lifetime becomes shorter with increasing excitation intensity.

The TA intensity and effective lifetime are summarized in Figure 4b. The TA intensity just after the excitation ($\sim$2 ps) linearly depends on the excitation intensity because the TA is proportional to the photocarrier density. On the other hand, the lifetime is inversely proportional to the excitation intensity. Note that we could not accurately characterize TA lifetimes longer than 2 ns because of the limited delay stage length. We calculated the TA lifetime using $B = 1.7 \times 10^{-10}$ s^{-1} cm^3; the results are shown by the dashed line in Figure 4b. This theoretical calculation reproduces the data well. Therefore, we can conclude that our TA results agree well with those of PL measurements and are consistent with our carrier recombination model as described by eqs 1a−1c.

Finally, we discuss the exciton and free-carrier models in $CH_3NH_3PbI_3$ perovskite semiconductors. The data in the literature for the exciton binding energy in $CH_3NH_3PbI_3$ range between 25 and 37 meV,[22] which is large enough that the excitonic effect should appear at room temperature.[23] However, no excitonic effects appear in near-band-edge optical spectra at room temperature.[15] In addition, as demonstrated in this study, recombination of free electrons and holes dominates the relaxation processes of photoexcited states. We believe that the exciton binding energy is actually much smaller than the thermal energy at room temperature. We think that this discrepancy comes from the fact that the reported binding energy was evaluated based on low-temperature experiments. Because of the phase transition at 160 K,[24] the room-temperature exciton binding energy can be significantly different from that at low temperatures, as theoretically predicted.[25]

dx.doi.org/10.1021/ja506624n | J. Am. Chem. Soc. 2014, 136, 11610−11613

In conclusion, we have studied the photocarrier recombination and relaxation dynamics of $CH_3NH_3PbI_3$ thin films by means of time-resolved PL and TA spectroscopy. We revealed that the PL intensity just after the excitation shows square dependence on the excitation intensity, meaning that the radiative recombination of free electrons and holes is dominant for PL processes and the exciton model is not appropriate at room temperature. This result suggests that the working principle (and therefore the optimal device structure) of the perovskite solar cells should be different from organic photovoltaics as well as conventional sensitized solar cells. Perovskite semiconductors are quite different from the organic semiconductors for photovoltaic applications whose recombination dynamics are usually dominated by excitons.[26] The estimated radiative recombination rate of $CH_3NH_3PbI_3$ is comparable to that of typical direct-gap semiconductors used in optoelectronic devices. Our findings provide deep insights into the fundamental optical processes in $CH_3NH_3PbI_3$, and such insights are essential for the further development of highly efficient solar cells and other optoelectronic devices based on halide perovskite semiconductors.

AUTHOR INFORMATION

Corresponding Authors

yamada.yasuhiro.6c@kyoto-u.ac.jp
kanemitu@scl.kyoto-u.ac.jp

Notes

The authors declare no competing financial interest.

ACKNOWLEDGMENTS

Part of this work was supported by the Sumitomo Electric Industries Group CSR Foundation (to Y.Y. and Y.K.), JST-PRESTO (to A.W.), and JST-CREST (to Y.K.). Prof. K. Matsuda (Kyoto University) is acknowledged for the SEM measurement.

REFERENCES

(1) (a) Kojima, A.; Teshima, K.; Shirai, Y.; Miyasaka, T. *J. Am. Chem. Soc.* **2009**, *131*, 6050. (b) Mitzi, D. B.; Wang, S.; Feild, C. A.; Chess, C. A.; Guloy, A. M. *Science* **1995**, *267*, 1473. (c) Ogawa, T.; Kanemitsu, Y. *Optical Properties of Low-dimensional Materials*; World Scientific: Singapore, 1995. (d) Kamat, P. V. *J. Am. Chem. Soc.* **2014**, *136*, 3713.

(2) Kim, H.-S.; Lee, C.-R.; Im, J.-H.; Lee, K.-B.; Moehl, T.; Marchioro, A.; Moon, S.-J.; Humphry-Baker, R.; Yum, J.-H.; Moser, J. E.; Grätzel, M.; Park, N.-G. *Sci. Rep.* **2012**, *2*, 591.

(3) Lee, M. M.; Teuscher, J.; Miyasaka, T.; Murakami, T. N.; Snaith, H. J. *Science* **2012**, *338*, 643.

(4) Park, N.-G. *J. Phys. Chem. Lett.* **2013**, *4*, 2423.

(5) Burschka, J.; Pellet, N.; Moon, S.-J.; Humphry-Baker, R.; Gao, P.; Nazeeruddin, M. K.; Grätzel, M. *Nature* **2013**, *499*, 316.

(6) Chen, Q.; Zhou, H.; Hong, Z.; Luo, S.; Duan, H.-S.; Wang, H.-H.; Liu, Y.; Li, G.; Yang, Y. *J. Am. Chem. Soc.* **2014**, *136*, 622.

(7) Xing, G.; Mathews, N.; Lim, S. S.; Yantara, N.; Liu, X.; Sabba, D.; Grätzel, M.; Mhaisalkar, S.; Sum, T. C. *Nat. Mater.* **2014**, *13*, 476.

(8) Deschler, F.; Price, M.; Pathak, S.; Klintberg, L. E.; Jarausch, D.-D.; Higler, R.; Hüttner, S.; Leijtens, T.; Stranks, S. D.; Snaith, H. J.; Atatüre, M.; Phillips, R. T.; Friend, R. H. *J. Phys. Chem. Lett.* **2014**, *5*, 1421.

(9) Liu, M.; Johnston, M. B.; Snaith, H. J. *Nature* **2013**, *501*, 395.

(10) Service, R. F. *Science* **2014**, *344*, 458.

(11) National Renewable Energy Laboratory, "Research Cell Efficiency Records" [http://www.nrel.gov/ncpv/images/efficiency_chart.jpg].

(12) Stranks, S. D.; Eperon, G. E.; Grancini, G.; Menelaou, C.; Alcocer, M. J. P.; Leijtens, T.; Herz, L. M.; Petrozza, A.; Snaith, H. J. *Science* **2013**, *342*, 341.

(13) Xing, G.; Mathews, N.; Sun, S.; Lim, S. S.; Lam, Y. M.; Grätzel, M.; Mhaisalkar, S.; Sum, T. C. *Science* **2013**, *342*, 344.

(14) (a) Giorgi, G.; Fujisawa, J.-I.; Segawa, H.; Yamashita, K. *J. Phys. Chem. Lett.* **2013**, *4*, 4213. (b) Heo, J. H.; Im, S. H.; Noh, J. H.; Mandal, T. N.; Lim, C.-S.; Chang, J. A.; Lee, Y. H.; Kim, H.-J; Sarkar, A.; Nazeeruddin, M. K.; Grätzel, M.; Seok, S. I. *Nat. Photonics* **2013**, *7*, 486.

(15) Kirchartz, T.; Mattheis, J.; Rau, U. *Phys. Rev. B* **2008**, *78*, 235320.

(16) Yamada, Y.; Nakamura, T.; Endo, M.; Wakamiya, A.; Kanemitsu, Y. *Appl. Phys. Express* **2014**, *7*, 032302.

(17) (a) Yamada, Y.; Kanemitsu, Y. *Appl. Phys. Lett.* **2012**, *101*, 133907. (b) Phuong, L. Q.; Okano, M.; Yamada, Y.; Nagaoka, A.; Yoshino, K.; Kanemitsu, Y. *Appl. Phys. Lett.* **2013**, *103*, 191902.

(18) Wakamiya, A.; Endo, M.; Sasamori, T.; Tokitoh, N.; Ogomi, Y.; Hayase, S.; Murata, Y. *Chem. Lett.* **2014**, *43*, 711.

(19) (a) Yasuda, H.; Kanemitsu, Y. *Phys. Rev. B* **2008**, *77*, 193202. (b) Yamada, Y.; Yasuda, H.; Tayagaki, T.; Kanemitsu, Y. *Phys. Rev. Lett.* **2009**, *102*, 247401.

(20) (a) Varshni, Y. P. *Phys. Status Solidi* **1967**, *19*, 459. (b) Dmitriev, A.; Oruzheinikov, A. *J. Appl. Phys.* **1999**, *86*, 3241.

(21) (a) Even, J.; Pedesseau, L.; Dupertuis, M.-A.; Jancu, J.-M.; Katan, C. *Phys. Rev. B* **2012**, *86*, 205301. (b) Even, J.; Pedesseau, L.; Jancu, J.-M.; Katan, C. *J. Phys. Chem. Lett.* **2013**, *4*, 2999.

(22) Wehrenfennig, C.; Liu, M.; Snaith, H. J.; Johnston, M. B.; Herz, L. M. *J. Phys. Chem. Lett.* **2014**, *5*, 1300 and references therein.

(23) Yu, P. Y.; Candona, M. *Fundamentals of Semiconductors*, 3rd ed.; Springer: New York, 2001.

(24) Onoda-Yamamuro, N.; Matsuo, T.; Suga, H. *J. Phys. Chem. Solids* **1990**, *51*, 1383.

(25) Even, J.; Pedesseau, L.; Katan, C. *J. Phys. Chem. C* **2014**, *118*, 11566.

(26) Menke, S. M.; Holmes, R. J. *Energy Environ. Sci.* **2014**, *7*, 499.